the FEBS Journal
EDITOR'S CHOICE

N-terminally extended analogues of the K^+ channel toxin from *Stichodactyla helianthus* as potent and selective blockers of the voltage-gated potassium channel Kv1.3

Shih C. Chang[1], Redwan Huq[2], Sandeep Chhabra[1], Christine Beeton[2], Michael W. Pennington[3], Brian J. Smith[4] and Raymond S. Norton[1]

1 Medicinal Chemistry, Monash Institute of Pharmaceutical Sciences, Monash University, Parkville, Vic., Australia
2 Department of Molecular Physiology and Biophysics, Baylor College of Medicine, Houston, TX, USA
3 Peptides International, Louisville, KY, USA
4 Department of Chemistry and Physics, La Trobe Institute for Molecular Science, La Trobe University, Melbourne, Vic., Australia

Keywords
electrophysiology; molecular dynamics; N-terminal extension; potassium channels; ShK

Correspondence
R. S. Norton, Medicinal Chemistry, Monash Institute of Pharmaceutical Sciences, Monash University, Parkville, Vic. 3052, Australia
Fax: +613 990 39582
Tel: +61 3 9903 9167
E-mail: ray.norton@monash.edu

(Received 27 August 2014, revised 22 March 2015, accepted 6 April 2015)

doi:10.1111/febs.13294

The voltage-gated potassium channel Kv1.3 is an important target for the treatment of autoimmune diseases and asthma. Blockade of Kv1.3 by the sea anemone peptide K^+-channel toxin from *Stichodactyla helianthus* (ShK) inhibits the proliferation of effector memory T lymphocytes and ameliorates autoimmune diseases in animal models. However, the lack of selectivity of ShK for Kv1.3 over the Kv1.1 subtype has driven a search for Kv1.3-selective analogues. In the present study, we describe N-terminally extended analogues of ShK that contain a negatively-charged Glu, designed to mimic the phosphonate adduct in earlier Kv1.3-selective analogues, and consist entirely of common protein amino acids. Molecular dynamics simulations indicated that a Trp residue at position [-3] of the tetrapeptide extension could form stable interactions with Pro377 of Kv1.3 and best discriminates between Kv1.3 and Kv1.1. This led to the development of ShK with an N-terminal Glu-Trp-Ser-Ser extension ([EWSS]ShK), which inhibits Kv1.3 with an IC_{50} of 34 pM and is 158-fold selective for Kv1.3 over Kv1.1. In addition, [EWSS]ShK is more than 2900-fold more selective for Kv1.3 over Kv1.2 and KCa3.1 channels. As a highly Kv1.3-selective analogue of ShK based entirely on protein amino acids, which can be produced by recombinant expression, this peptide is a valuable addition to the complement of therapeutic candidates for the treatment of autoimmune diseases.

Introduction

Almost 70 different autoimmune diseases are known, affecting millions of people worldwide [1,2]. Autoimmune diseases are among the top ten leading causes of death in women below 65 years of age [3], and involve various organs in the body, such as the joints [rheumatoid arthritis (RA)], heart, lungs, central nervous system [multiple sclerosis (MS)], endocrine organs (type 1 diabetes mellitus) and skin (psoriasis). Tissue destruction in these diseases is mediated in part by self-reactive T lymphocytes. As T cells undergo

Abbreviations
[EESS]ShK, ShK with an N-terminal Glu-Glu-Ser-Ser extension; [ESSS]ShK, ShK with an N-terminal Glu-Ser-Ser-Ser extension; [EWSS]ShK, ShK with an N-terminal Glu-Trp-Ser-Ser extension; Kv, voltage-gated K^+ channel; MD, molecular dynamics; MgTx, margatoxin; MS, multiple sclerosis; Ppa, para-phosphono-phenylalanine; pTyr, phospho-tyrosine; RA, rheumatoid arthritis; ShK, K^+ -channel toxin from *Stichodactyla helianthus*; T_{EM}, effector memory T (lymphocyte).

repeated antigen stimulation, they differentiate into terminally differentiated effector memory T (T_{EM}) cells [4,5], which are characterized by high expression of the voltage-gated potassium channel Kv1.3 after activation and the absence of both the chemokine receptor CCR7 and phosphatase CD45RA on their surface [6]. The disease-associated T cells in patients with MS (specific for myelin antigens), type 1 diabetes mellitus (specific for GAD65 antigens), RA (synovial T cells), psoriasis and asthma (induced-sputum T cells) are T_{EM} effector cells [6–15]. In addition, B cells differentiate into class-switched B cells upon recurring antigen stimulation and are also implicated in MS [16] and other autoimmune diseases; these cells are a major source of IgG autoantibodies that result in direct tissue damage in MS [17,18], type 1 diabetes mellitus [19] and RA [20]. Similar to T_{EM} cells, class-switched B cells upregulate Kv1.3 upon activation and their proliferation can be suppressed through the inhibition of Kv1.3 channels [6,21]. On the other hand, $CCR7^+$ naïve and central memory cells are less sensitive to the inhibition of Kv1.3 because they upregulate KCa3.1 channels upon activation [6], as do naïve and IgD^+CD27^+ memory B cells, which are also not sensitive to Kv1.3 blockers [21]. Consequently, selective blockers of Kv1.3 are expected to reduce the severity of autoimmune diseases without inducing generalized immunosuppression [22,23].

Recently, blocking Kv1.3 was shown to have additional therapeutic potential. Blocking Kv1.3 with margatoxin (MgTx) increased the differentiation of neural progenitor cells into neurones and enhanced neurone-regeneration [24]. In addition, inhibition of Kv1.3 with peptides such as the sea anemone peptide K^+-channel toxin from *Stichodactyla helianthus* (ShK), as well as the scorpion toxins MgTx and charybdotoxin, blocked the proliferation of $CD8^+$ cytotoxic effector memory T cells and their secretion of granzyme B, which is toxic to the neuronal cells [25]. Intriguingly, the toxicity of granzyme B was found to be mediated partially through Kv1.3 [26]. These findings indicate that Kv1.3 is not only an attractive therapeutic target for immunomodulation, but also plays an important role in neurone protection. Recent results also suggest that Kv1.3 suppression may be useful in the treatment of ulcerative colitis [27].

One of the most potent inhibitors of Kv1.3 is the sea anemone toxin ShK, which blocks Kv1.3 with an IC_{50} of 11 pM [28]. ShK is a 35-residue polypeptide stabilized by three disulfide bridges and consists of two short α-helices comprising residues 14–19 and 21–24 [29]. ShK interacts with all four subunits of the Kv1.3 channel tetramer, with Lys22 occluding the channel pore [28,30,31]. ShK and its analogues have been shown to suppress proliferation of T_{EM} cells [6] and to improve the condition of two animal models of MS (chronic relapse-remitting and adoptive experimental autoimmune encephalomyelitis) [7,32], the pristane-induced arthritis model of RA, as well as animal models of asthma and psoriasis [10,33].

Although ShK has great therapeutic potential, it also binds to the closely-related Kv1 subtype Kv1.1 (K_D = 16 pM), which is found in the heart and central nervous system [34] where it plays an essential role in the control of neurone excitability [35]. In addition, it was found that most neuronal heterotetrameric Kv1 channels contain at least one Kv1.1 and/or Kv1.2 subunit [36,37] and knockout of Kv1.1 or Kv1.2 in mice resulted in seizures during early development [35,38,39]. Kv1.1-deficient mice were also found to exhibit cardiac dysfunction associated with severe epileptic activity [40]. In humans, the loss-of-function gene mutations of Kv1.1 can cause epilepsy, episodic ataxia and involuntary muscular contractions [41–43]. To avoid potential cardiac and neurotoxicity associated with Kv1.1 and/or Kv1.2 inhibition, highly Kv1.3-selective analogues are desirable, especially in patients with MS whose blood–brain barrier is compromised, with an increased potential for peptides and proteins to gain entry into the central nervous system [44].

Several analogues of ShK with enhanced Kv1.3-selectivity have been synthesized, although they include nonprotein extensions to their N-terminus [45,46]. One such analogue, ShK-186, which has recently entered clinical trials for the treatment of a range of autoimmune diseases, contains an N-terminal phospho-tyrosine (pTyr) and a C-terminal amide; the latter was introduced to avoid carboxypeptidase degradation and has no effect on binding affinity [47]. This analogue, however, is rapidly dephosphorylated *in vivo* [47], and induces low titre anti-ShK-186 antibody production [7]. Another analogue, ShK-192, differs from ShK-186 by the replacement of a methionine (Met21) with norleucine to reduce the potential for oxidative metabolism, and the replacement of the phospho moiety with a nonhydrolyzable phosphono group [para-phosphono-phenylalanine (Ppa)]. ShK-192 has slightly lower affinity for Kv1.3 but significantly improved selectivity over Kv1.1; it is predicted to bind to the extracellular face of the channel, with the terminal negatively-charged phosphono group forming a salt bridge with the side-chain ammonium group of Lys411 in Kv1.3 [46]. In the present study, we employed computational techniques to design analogues of ShK-192 with high selectivity for Kv1.3 over Kv1.1. Molecular modelling

suggested that extension of the N-terminus of ShK with the tetrapeptide sequence ESSS could mimic the phosphono moiety in ShK-192. Further MD simulations suggested that Trp at position [-3] would be favourable in forming stable interaction with Pro377 of Kv1.3, and the results were validated by electrophysiology studies. This analogue, ShK with an N-terminal Glu-Trp-Ser-Ser extension ([EWSS]ShK), was also tested against KCa3.1 and Kv1.2 channels, which are common targets for toxins that have strong affinity for Kv1.3, such as Vm24, OSK1 analogue and MgTx [48–50]. Overall, three analogues were designed and either synthesized or expressed. Electrophysiology results showed that [EWSS]ShK retains high potency against Kv1.3, with an IC_{50} of 34 pM. Moreover, it is 158-fold selective for Kv1.3 over Kv1.1 and more than 2900-fold selective for Kv1.3 over Kv1.2 and KCa3.1.

Results

Modelling of N-terminal extensions to ShK

In a model of ShK-192 bound to Kv1.3 that we had developed previously [46], the N-terminal negatively-charged phosphono group was predicted to form a salt bridge with the side-chain ammonium group of Lys411 of Kv1.3. Although the phosphono group presumably contributed to the high affinity of this analogue for the channel, it also represents a potential immunogenicity liability, and requires chemical synthesis for its production and attachment to the peptide; these issues can be overcome by using common protein amino acids in place of the phosphono group. In the homology model of Kv1.3 in complex with ShK-192 (Fig. 1A), the phosphono group lies ~ 8 Å from the native toxin N-terminus (Fig. 1B), which is almost twice the distance between the N-terminus and the carboxylate of a fully-extended Glu residue (~ 4.7 Å). It is therefore likely that more than a single amino acid would be required to replace the phosphono group and its linker to span the required distance and maintain affinity for the channel.

Homology models of ShK-192 analogues with the phosphono group and linker replaced with an N-terminal Glu with 0, 1 or 2 intervening Ser residues were therefore created using MODELLER [51]; Ser residues were chosen to assist in maintaining the solubility and approximately mimic the properties of the mini-PEG spacer in ShK-192. Models with the Glu residue appended directly to the native toxin N-terminus could be generated such that the carboxylate of the Glu[-1] could form a salt bridge with the side-chain ammonium of Lys411 of the channel. However, these models could not be energetically differentiated from other models in which the salt bridge was absent (Fig. 1C); thus, with a Glu residue appended directly to the N-terminus of native ShK the distance between the carboxylate of the Glu extension and ammonium of Lys411 ranged from 2.9 Å to 17.4 Å, although the energy varied only over a very narrow range (−76 to −103 $kJ \cdot mol^{-1}$), indicating little preference toward forming the salt bridge in these models. Similarly, with one or two intervening Ser residues, models could be generated with the necessary salt bridge but, once again, these models were not significantly lower in energy than models in which the salt bridge was absent. With three intervening Ser residues, yielding an ESSS extension, the lowest energy models preserved the required interaction between the N-terminal Glu[-4] carboxylate and the ammonium of Lys411 of the channel.

In the lowest-energy model of ShK with an N-terminal Glu-Ser-Ser-Ser extension ([ESSS]ShK) (Fig. 1D), apart from the salt bridge between Glu[-4] and Lys411, the only other interaction of the extension with the channel is the side chain of Ser[-3] with Pro377; the other Ser extension residues (at positions [-1] and [-2]) project outwardly to the solvent.

Structure–activity relationship exploration at the N-terminus and modelling of [EWSS]ShK

The design of a Kv1.3-selective analogue exploited the amino acid sequence variation between Kv1.3 and Kv1.1 (Fig. 2). The two channels are highly homologous and differ in only seven surface-exposed residues, with most of these differences being conservative substitutions; for example, Asp375 in Kv1.3 to Glu in Kv1.1 (D375E). The other differences are D376E, P377A, S378E, G380H, N382S and H404Y (Fig. 1A); of these, the first four residues lie in the turret between the S5 and pore helices, whereas His404 lies in the loop connecting the pore and S6 helices. Moreover, mouse and human Kv1.3 are very similar, with the only differences in surface-exposed residues between mouse and human being S378T and N382S; the sequences of mouse and human Kv1.1 are identical across the transmembrane and selectivity filter regions.

Of the seven surface residue differences between Kv1.3 and Kv1.1, only Pro377 of Kv1.3 contacts Ser[-3] of the N-terminal extension of [ESSS]ShK in the model of the complex. The hydrophobic side chains of Ile, Leu and Val are all observed to interact favourably with the side chain of Pro [52], although the binding affinity with Pro relative to Ala is likely to be context-dependent (i.e. whether the side chains are sol-

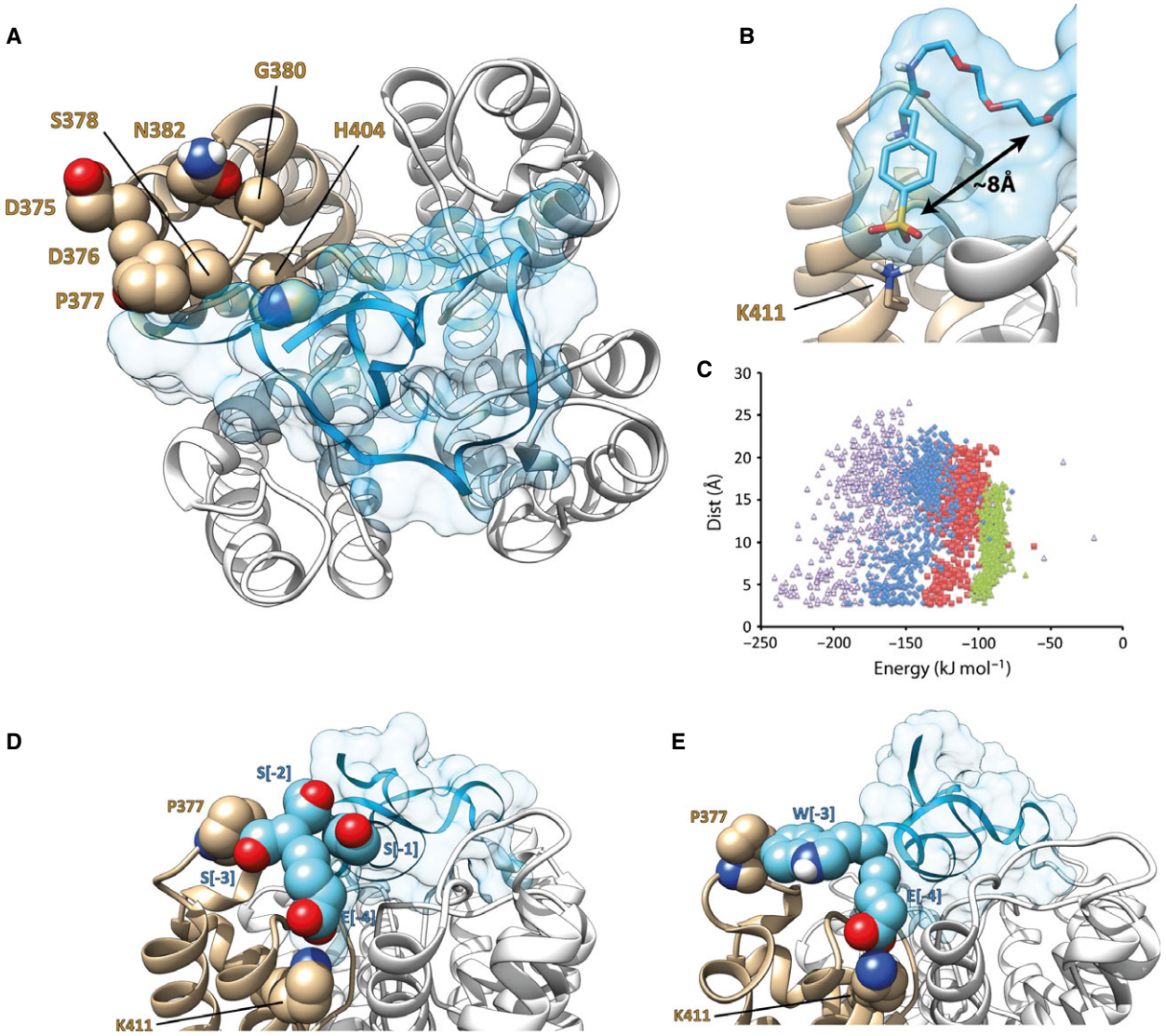

Fig. 1. Homology modelling of ShK analogues in complex with Kv1.3. (A) ShK-192 in complex with Kv1.3; view perpendicular to the membrane plane with the channel represented as a white and tan ribbon, and the ShK analogue in blue with a transparent surface. The side-chain atoms of residues on the surface of the channel that differ between Kv1.1 and Kv1.3 are illustrated as spheres (atom colouring with carbon tan). (B) The phosphono group of the N-terminal Ppa extension in ShK-192 lies ~ 8 Å from the N-terminus of the native ShK and forms a salt bridge with the ammonium of Lys411. (C) Comparison of MODELLER energies and separation between the N-terminal Glu of the ShK analogue and Lys411 of the channel. Extensions to ShK of 1 (green triangle; E), 2 (red square; ES), 3 (blue diamond; ESS) and 4 (purple triangle; ESSS) residues. (D) Homology model of [ESSS]ShK in complex with Kv1.3. The side-chain atoms of Pro377 and Lys411 of the channel are represented as spheres (atom colouring with carbon tan). The side-chain atoms of the four-residue extension, ESSS, are represented as spheres (atom colouring with carbon cyan). (E) Homology model of [EWSS]ShK in complex with Kv1.3. The side-chain atoms of Pro377 and Lys411 of the channel are highlighted. The side-chain atoms of the first two residues (EW) of the four-residue extension are represented as spheres (atom coloring with carbon cyan).

```
                   ******************** *****     * * ********** ********* ************************************
Kv1.1 ELGLLIFFLFIGVILFSSAVYFAEAEEAESHFSSIPDAFWWAVVSMTTVGYGDMYPVTIGGKIVGSLCAIAGVLTIALPVPVIVSNFNYFY
Kv1.3 ELGLLIFFLFIGVILFSSAAYFAEADDPSSGFNSIPDAFWWAVVTMTTVGYGDMHPVTIGGKIVGSLCAIAGVLTIALPVPVIVSNFNYFY
```

Fig. 2. Sequence alignment of the transmembrane regions of Kv1.1 and Kv1.3. Annotation highlights conservation between Kv1.1 (residues 325–415) and Kv1.3 (residues 350–440) sequences (asterisks = conserved); surface-exposed residues that differ between the two sequences are highlighted in yellow, residues in the selectivity filter are highlighted in green; shaded areas indicate helices.

vent exposed or buried in the interior of the protein) [53]. The side chain of Trp, however, is predicted to interact more tightly with the side chain of Pro than Ala, independent of its environment; moreover, Trp exhibits the largest affinity for Pro of all 20 commonly occurring protein amino acids, and should thus best differentiate between Kv1.3 and Kv1.1.

Based on these observations, Ser[-3] of [ESSS]ShK was replaced with Trp and the resulting model subjected to molecular dynamics (MD) simulation. The final model, after 1.0 ns of MD, is presented in Fig. 1E. The side chain of Trp[-3] of the ShK analogue is predicted to interact with that of Pro377 of Kv1.3, at the same time as maintaining the interaction of the Glu[-4] carboxylate with Lys411. The side-chain hydroxyl of Ser[-1] is also predicted to form a hydrogen bond with the carboxylate of Asp433 of an adjacent channel monomer (a residue conserved between Kv1.3 and Kv1.1), further stabilizing the complex.

MD simulations of the ShK derivatives [ESSS]ShK, [EISS]ShK, [ELSS]ShK and [EVSS]ShK (data not shown) indicated that the side chains of Ser[-3], Ile[-3], Leu[-3] and Val[-3], respectively, did not form stable interactions with the alkane side chain of Pro377 (the loop containing Pro377 moved away from the extension during the simulation), suggesting that a larger side-chain group (such as the indole group in tryptophan) is necessary to span the distance. The salt bridge between the carboxylate of Glu[-4] and Lys411 could be maintained throughout the simulations.

MD simulations of ShK with an N-terminal Glu-Glu-Ser-Ser extension ([EESS]ShK) (data not shown), in which Ser[-3] was replaced with Glu, in complex with Kv1.3 resulted in the Glu[-3] also disengaging from its initial association with Pro377, although, again, the salt bridge between the carboxylate of Glu[-4] and Lys411 could be maintained with the alkane face of the side chain of Glu[-3] packing against the alkane side chains of the invariant channel residues Val406 and Thr407. Overall, the tetrapeptide extension EWSS best captures the structural and physicochemical properties of the Ppa moiety on ShK-192 in comparison to other N-terminal amino acid extensions (Fig. 3).

Synthesis of [ESSS]ShK and [EESS]ShK

Peptides were assembled using standard Fmoc-tBu solid-phase peptide synthesis. The crude product was oxidized using glutathione-mediated oxidative folding conditions that have been used successfully for many other ShK analogues [54]. The peptides folded rapidly, resulting in the typical pattern of a major earlier-eluting peak by RP-HPLC followed by later-eluting misfolded and side-product species. [ESSS]ShK and [EESS]ShK were purified to homogeneity by preparative RP-HPLC. Each peptide had the correct mass by ESI-MS (data not shown), demonstrating that the three disulfide bonds had been formed. The yield was ~ 16% of the theoretical yield based upon the amount of starting resin for each of the peptides.

Expression and purification of [EWSS]ShK

The solubilized His-tagged fusion protein was denatured and loaded onto an nitrilotriacetic acid column, and the bound protein was refolded by gradual removal of denaturant. The eluted fusion protein was then cleaved with enterokinase and purified to homogeneity by RP-HPLC. Analytical RP-HPLC (Fig. 4A)

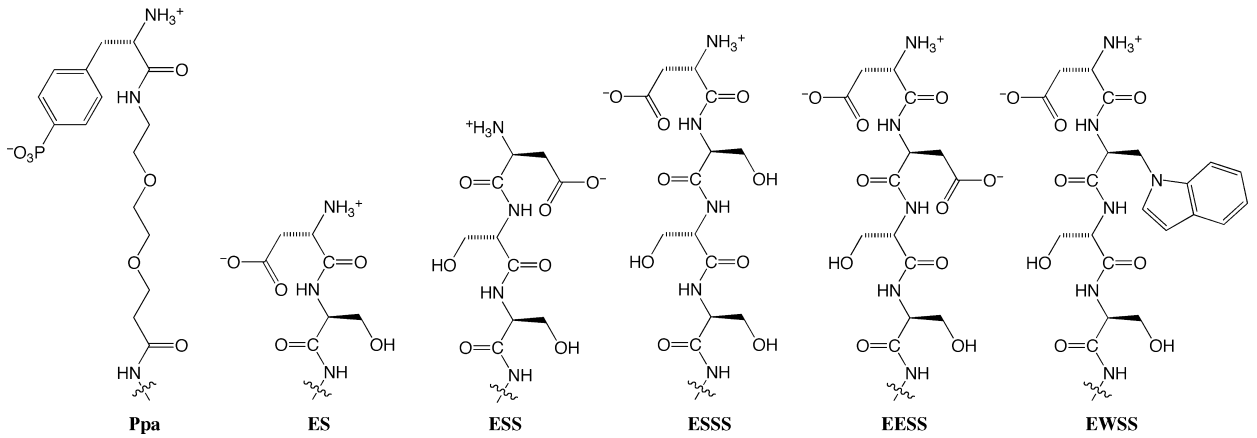

Fig. 3. N-terminal extensions of ShK analogues. Schematic illustrating the structural similarity and physicochemical properties of Ppa moiety of ShK-192 and various amino acid extensions.

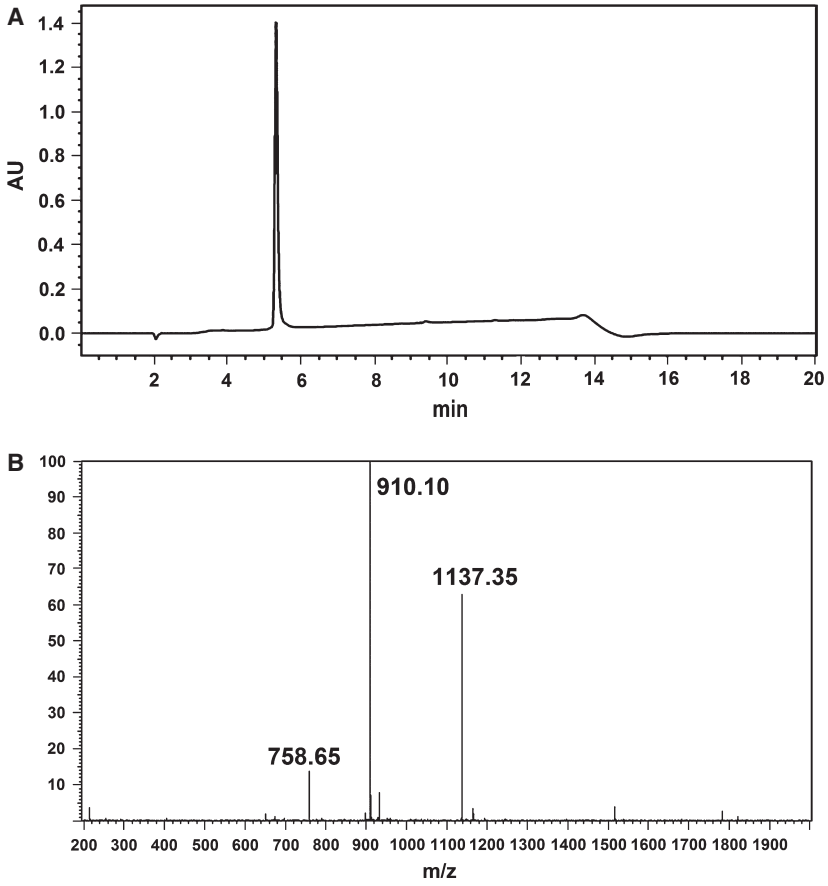

Fig. 4. Purification and characterization of [EWSS]ShK. (A) Analytical RP-HPLC chromatograph for the final purified [EWSS]ShK with absorbance at 214 nm with purity ≥ 95%. (B) ESI-MS analysis of [EWSS]ShK. The multicharged ions are deconvoluted to a molecular mass of 4544 Da, which is consistent with the theoretical mass.

showed that the purified ShK analogue was essentially homogenous. High-resolution electrospray ionization time-of-flight MS analysis (Fig. 4B) of [EWSS]ShK produced a mean molecular mass of 4544 Da; this value was identical to the theoretical molecular mass of 4544 Da for [EWSS]ShK toxin with all six cysteine residues engaged in the three native disulfide bonds [55]. The yield of [EWSS]ShK was ~ 2 mg·L^{-1}.

K^+ -channel blocking activity

Well-established whole-cell patch clamp electrophysiology assays were conducted to determine the potency and selectivity of [ESSS]ShK, [EESS]ShK and [EWSS]ShK on Kv1.3 and Kv1.1 (Fig. 5A). [ESSS]ShK inhibited Kv1.3 with an IC_{50} of 657 ± 79 pM, and with lower affinity towards Kv1.1, with an IC_{50} of 1327 ± 386 pM, making it two-fold selective for Kv1.3 over Kv1.1. [EESS]ShK exhibited slightly higher affinity than [ESSS]ShK towards Kv1.3, with an IC_{50} of 311 ± 41 pM, and an IC_{50} of 830 ± 116 pM for Kv1.1. [EESS]ShK is 2.1-fold higher in affinity for Kv1.3 compared to [ESSS]ShK (Fig. 5B and Table 1), and also 2.7-fold selective for Kv1.3 over Kv1.1. Thus, both analogues have reduced affinity for K^+ channels and do not discriminate well between Kv1.3 and Kv1.1, exhibiting similar selectivity as ShK. The implication is that neither Ser[-3] nor Glu[-3] was able to discriminate between Pro377 in Kv1.3 and Ala in Kv1.1.

Recombinant [EWSS]ShK, however, exhibited high affinity for Kv1.3, with an IC_{50} of 34 ± 8 pM for mKv1.3 but significantly reduced affinity (IC_{50} = 5371 ± 912 pM) for Kv1.1 (Fig. 5 and Table 1) with a Hill coefficient of 1 (Table 2). Moreover, [EWSS]ShK exhibited only weak affinity for Kv1.2 (IC_{50} > 100 nM) and KCa3.1 (IC_{50} > 100 nM) (Fig. 6 and Table 1). Thus, [EWSS]ShK shows a similar level of selectivity for Kv1.3 as ShK-192 but with four-fold higher affinity.

Discussion

To develop selective peptide blockers of Kv1.3, one approach is to map the binding sites of the peptide for the related channel and modify residues at those sites. Previously, in an effort to detect high expression of Kv1.3 on T_{EM} cells by flow cytometry, a fluorescein

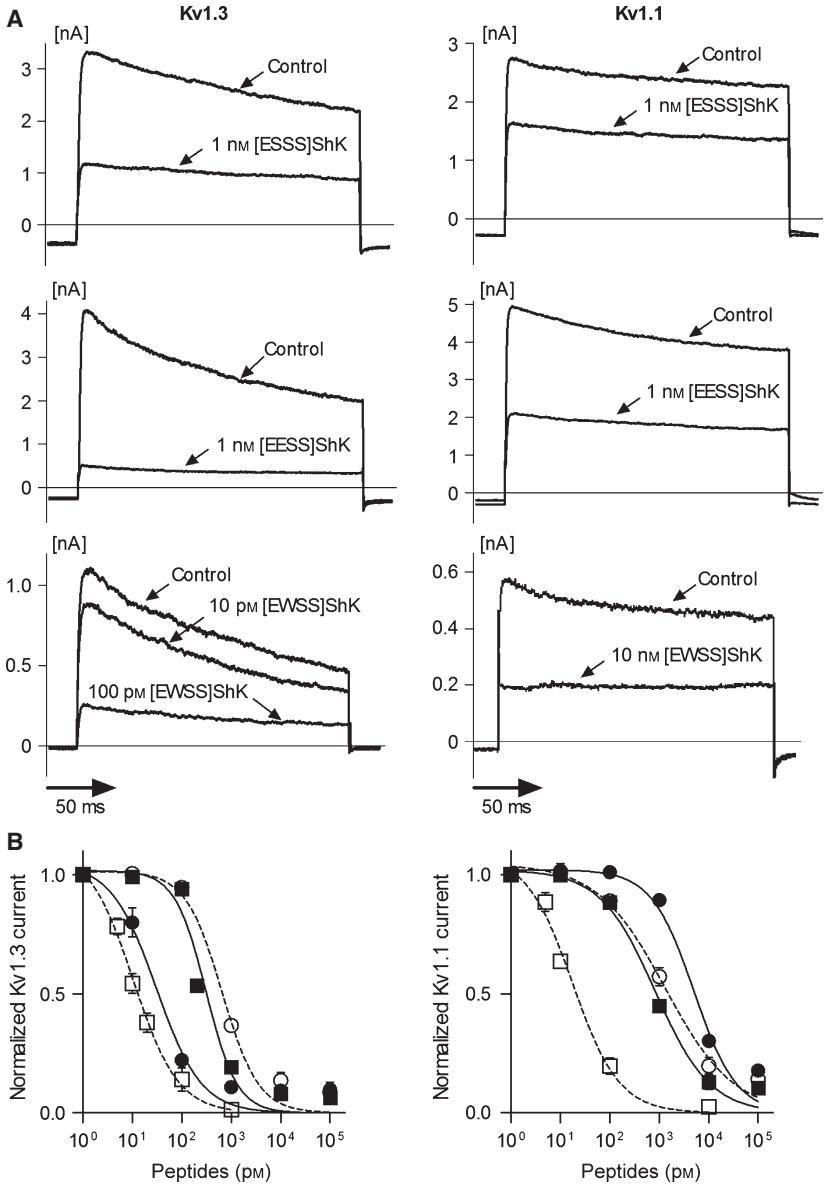

Fig. 5. Selectivity of N-terminally extended ShK analogues. (A) Effect of [ESSS]ShK (top), [EESS]ShK (middle) and [EWSS]ShK (bottom) on Kv1.3 and Kv1.1 currents. (B) Effects of [ESSS]ShK (○, dotted line), [EESS]ShK (■, solid line), [EWSS]ShK (●, solid line) and ShK (□, dotted line) on Kv1.3 or Kv1.1 currents measured by whole-cell patch-clamp on L929 fibroblasts stably transfected with mKv1.3 or mKv1.1, respectively, and fitted to a Hill equation (n = 3–5 cells per concentration). Left: whole-cell Kv1.3 currents. Right: whole-cell Kv1.1 currents. Data are reported as the mean ± SEM.

moiety (F6CA) was attached to the N-terminus of ShK through an 11-atom linker (amino-ethyloxy-ethyloxy-acetic acid); the linker was introduced to reduce steric effects caused by the bulky F6CA moiety. The fluorescent analogue ShK-F6CA exhibited 70-fold selectivity for Kv1.3 over the closely-related Kv1.1 [45]. In subsequent studies, the fluorophore was replaced with pTyr to mimic the bulk and negative charge of the fluorophore, generating ShK-186, which displayed 100-fold selectivity for Kv1.3 over Kv1.1 and more than 700-fold selectivity over all other channels tested, at the same time as maintaining picomolar potency on Kv1.3 [32]. ShK-186 does not delay clearance of rat-adapted influenza virus or *Chlamydia trachomatis* in rats and does not affect tumour killing by all subsets of human natural killer lymphocytes, demonstrating that it does not compromise the normal function of the immune system, and its ability to fight an acute infection or tumour formation [10,56]. However, the pTyr on ShK-186 is rapidly dephosphorylated in serum, and the nine-atom linker dictates that it has to be synthesized and cannot be produced recombinantly. Although replacement of pTyr by another uncommon amino acid led to the generation of ShK-192 with potentially increased immunogenicity, its *in vivo* effectiveness was moderately reduced [46]. To overcome these potential shortcomings, we have developed new Kv1.3-selective

Table 1. Binding affinities (IC_{50}, pM) of ShK analogues.

	Peptide (pM)					
Channel	ShK [28, 31]	ShK-186 [46]	ShK-192 [46]	[ESSS]ShK	[EESS]ShK	[EWSS]ShK
Kv1.1	18 ± 3	6900 ± 500	22 000 ± 3000	1327 ± 386 (4)	830 ± 116 (5)	5371 ± 912 (4)
Kv1.2	900 ± 300	ND	ND	ND	ND	> 100 000 (4)
Kv1.3	11 ± 2	71 ± 4	140 ± 19	657 ± 79 (4)	311 ± 41 (4)	34 ± 8 (3)
KCa3.1	30 000 ± 7000	ND	> 100 000 ± 700	ND	ND	> 100 000 (3)
Kv1.1/Kv1.3	16	97	157	2.0	2.7	158

Data are the mean ± SEM. Numbers in parenthesis are the number of cells tested for each blocker and channel.

Table 2. Hill coefficients for ShK analogues for Kv1.1 and Kv1.3 channels and are determined by fitting the dose–response curves to the Hill equation.

	Kv1.3	Kv1.1
[ESSS]ShK	−1.2 ± 0.2	−0.6 ± 0.1
[EESS]ShK	−1.4 ± 0.2	−0.8 ± 0.1
[EWSS]ShK	−1.0 ± 0.2	−1.0 ± 0.1
ShK	−1.0 ± 0.1	−0.9 ± 0.1

Data are the mean ± SEM.

analogues consisting of only common protein amino acids, with the prospect of being developed as a new therapeutic for the treatment of autoimmune diseases.

Advanced MD simulations led to our design of a highly Kv1.3-selective ShK analogue, [EWSS]ShK, which is composed only of commonly-occurring protein amino acids and could be expressed recombinantly. This analogue is not susceptible to hydrolysis by phosphatases and exhibits only weak inhibition of Kv1.1, Kv1.2 and KCa3.1, at the same time as maintaining high potency against Kv1.3 (IC_{50} = 34 ± 8 pM). Our modelling studies suggest that the tetrapeptide extension can mimic the interactions with Kv1.3 predicted for the phosphono moiety and hydrophilic linker in ShK-192. Because [EWSS]ShK binds to Kv1.3, Glu[-4] of the N-terminal extension is predicted to engage in an electrostatic interaction with channel residue Lys411. A Trp residue adjacent to the terminal Glu was predicted to interact more favourably with the side chain of Pro377 compared to the equivalent Ala side chain in Kv1.1, which offers an explanation for the observed selectivity of [EWSS]ShK for Kv1.3. MD simulations of other ShK derivatives investigated in the present study showed that extensions with side chains of Ser[-3], Ile[-3], Leu[-3] and Val[-3] did not form a stable interaction with Pro377, explaining the observed lower affinity for Kv1.3 channel. In the case of [EESS]ShK, the alkane region of the side chain of Glu[-3] was found to pack against the alkane side chains of the channel invariant residues Val406 and Thr407, which explains the observed increase in the affinity of [EESS]ShK over [ESSS]ShK and the lack of increased selectivity.

Recently, we have developed another Kv1.3-selective analogue, [K18A]ShK, by substituting Lys18 to an Ala based on predictions from free-energy simulations [57]. The analogues [K18A]ShK and [EWSS]ShK both inhibit Kv1.3 with IC_{50} of ~ 35 pM and their binding modes are preserved in the docked complex with Kv1.3. Therefore, [EWSS, K18A]ShK, which incorporates both modifications, may further improve the selectivity for Kv1.3 over Kv1.1, Kv1.2 and KCa3.1.

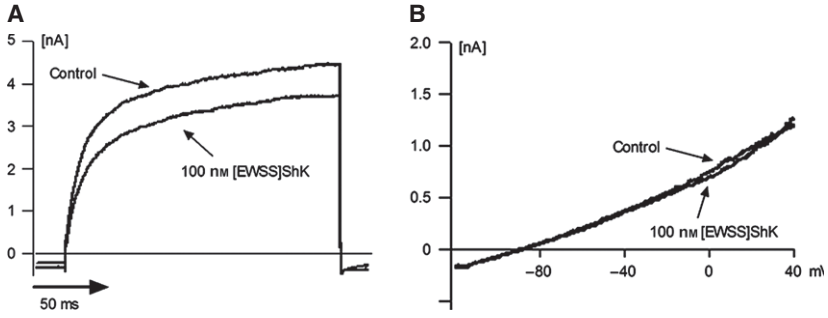

Fig. 6. Effects of [EWSS]ShK on Kv1.2 and KCa3.1. (A) The currents of Kv1.2 (left) and (B) KCa3.1 (right) were measured by whole-cell patch-clamp on B82 fibroblasts stably transfected with mKv1.2 or HEK293 cells stably transfected with hKCa3.1, respectively, and fitted to a Hill equation (n = 3–4 cells per concentration). All current traces were recorded at equilibrium block.

The presence of a Trp residue on the N-terminal extension confers practical advantages compared to native ShK, which lacks Trp. The Trp residue can be replaced with (4-Aza)Trp or (5-Aza)Trp [58], 5-hydroxytryptophan [59] or the recently developed (2, 7-Aza)Trp [60], which can be incorporated into bacterial expression, to be used as optical probes for assays in peptide delivery or to investigate Kv1.3 channel distribution in neuronal or cancer tissues.

In conclusion, the present study demonstrates that extension of the N-terminus of ShK with short peptide sequences based entirely on protein amino acids represents a viable strategy for generating potent and selective Kv1.3 blockers. These peptides can be produced by recombinant expression, which offers the prospect of reduced costs of production compared to previous synthetic analogues with additional chemical moieties, as well as the advantage of being classified as a biologic [61]. A Kv1.3-selective analogue that targets disease-associated T cells and class-switched B cells without compromising other immune cell subsets would have significant advantages over current therapies that cause cardiotoxicity or broad immunosuppression leading to severe infections or malignancies [62–64]. [EWSS]ShK is a promising lead in the development of such therapeutics.

Experimental procedures

Molecular modelling

Modelling of complexes of derivatives of ShK bound to Kv1.3 began with a model of ShK-192 bound to murine Kv1.3 that we had developed previously [46]. This model used the X-ray crystal structure of the K^+ channel from *Streptomyces lividans* (KcsA; PDBid 1BL8) as a template, to which was docked a model of ShK-192. Loop modelling of N-terminal extensions to ShK was performed using MODELLER [51]. For each complex, 25 initial models were created and, for each of these models, 25 loop models (consisting of the N-terminal extension residues only) were considered; a total of 625 models was created for each N-terminal extension length.

MD simulations of the complexes of [ESSS]ShK, [EESS]ShK, [EISS]ShK, [ELSS]ShK, [EVSS]ShK and [EWSS]ShK with mKv1.3 were performed using YASARA [65]; Ser[-3] of [ESSS]ShK (in complex with the channel) was mutated to Glu, Ile, Leu, Val or Trp, respectively. The complex was embedded into a membrane consisting only of phosphatidyl-ethanolamine extending ~ 15 Å beyond the solute in the membrane plane, and with water extending ~ 10 Å beyond the solute perpendicular to the membrane. Boundary conditions were set to periodic. Residues were ionized according to their expected state at pH 7.4. Sodium and chloride ions replaced water molecules to effect a final ionic concentration of 0.9%.

Standard AMBER03 force field parameters [66] were applied using a cut-off of 7.86 Å for all nonbonded interactions, whereas long-range Coulomb interactions were calculated using the particle-mesh Ewald algorithm. No restraints were applied, which required the use of a short time-step of 1.25 fs for intramolecular forces and 2.5 fs for intermolecular forces. All simulations were performed at a temperature of 298 K, maintained at a total pressure of 1 bar. An initial restrained equilibration simulation lasting 250 ps was applied to permit the lipid to pack around the solute without solvent interference. This was followed by 1.0 ns of unrestrained MD simulation.

Synthesis of [ESSS]ShK and [EESS]ShK

[EESS]ShK and [ESSS]ShK were synthesized on a Prelude peptide synthesizer (Protein Technologies, Inc., Tucson, AZ, USA) using an Fmoc-tBu strategy. The base peptide ShK was synthesized starting with Rink amide resin (Peptides International, Louisville, KY, USA). All couplings were mediated with diisopropyl carbodiimide and 6-chlorohydroxybenzotriazole. After completion of the 35-residue ShK sequence, the resin was divided into equal portions and the N-terminal extensions of EESS or ESSS were added to two separate aliquots. After solid-phase assembly of the linear peptide chain, the peptide was cleaved from the solid support and simultaneously deprotected using reagent K for 2 h at room temperature. The crude peptide was precipitated into ice-cold diethyl ether and washed thoroughly to remove cationic scavengers from the cleavage cocktail, dissolved in 50% aqueous acetic acid, then diluted in water and the pH adjusted to 8.0 with NH_4OH.

Disulfide bond formation was facilitated with reduced and oxidized glutathione in accordance with previously reported protocols for ShK [31]. The progress of folding was followed by RP-HPLC using a Phenomenex Luna C18 column (Phenomenex, Torrance, CA, USA) using a gradient of acetonitrile versus H_2O containing 0.05% trifluoroacetic acid from 10% to 70% over 35 min. Folding of the three disulfide bonds was also confirmed by the loss of six mass units from the crude material as determined by ESI-MS.

Expression and purification of [EWSS]ShK

The protocol was described in detail previously [67]. Briefly, [EWSS]ShK was expressed as thioredoxin fusion protein that forms inclusion bodies in BL21 (DE3). These were solubilized and refolded *in vitro*, cleaved with enterokinase and purified to homogeneity by RP-HPLC followed by lyophilization.

Electrophysiological analysis

L929 mouse fibroblast cells stably expressing mouse Kv1.1 or Kv1.3 channels [68] and B82 mouse fibroblast cells stably expressing mouse Kv1.2 were a kind gift from George Chandy (University of California, Irvine, CA, USA). HEK293 cells stably expressing human KCa3.1 were a kind gift from Khaled Houamed (University of Chicago, Chicago, IL, USA). Cells were studied using the whole-cell configuration of the patch-clamp technique at room temperature. Patch pipette resistances averaged 2–4 MΩ. Kv currents were recorded in bath solution that contained (in mM): 160 NaCl, 4.5 KCl, 2 $CaCl_2$, 1 $MgCl_2$, 10 Hepes, pH 7.2, 300 mOsm. Patch pipettes for recording Kv currents were filled with a solution containing (in mM): 145 KF, 10 Hepes, 10 EGTA, and 2 $MgCl_2$, pH 7.2, 290 mOsm. Kv currents were elicited by repeated 200-ms depolarizing pulses from a holding potential of −80 mV to 40 mV, applied every 30 s. KCa3.1 currents were recorded, as described previously [69] in bath solution containing (in mM): 160 Na^+ aspartate, 4.5 KCl, 2 $CaCl_2$, 1 $MgCl_2$, 5 Hepes, pH 7.4, 305 mOsm. Patch pipettes for recording KCa3.1 currents were filled with (in mM): 145 K^+ aspartate, 2 $MgCl_2$, 10 Hepes, 10 K_2EGTA, 8.5 $CaCl_2$ (1 μM free Ca^{2+}), pH 7.4, 295 mOsm. KCa3.1 currents were elicited by 200-ms voltage ramps from −120 mV to 40 mV, applied every 30 s. Peptides were diluted from 100 μM stock solutions into the appropriate bath solution and, after stable currents were recorded, the peptides were directly applied by perfusion with complete bath exchange in < 30 s. Steady-state change in peak current at 40 mV (Kv channels) or slope conductance measured at −80 mv (KCa channels) were recorded as a measure of channel block. The Port-a-Patch patch clamp system (Nanion Technologies, North Brunsiwck, NJ, USA) and NPC-1 chips with 2–3.5 MΩ resistance were also utilized in conjunction. IC_{50} values of the peptides were calculated by fitting the Hill equation steady-state current block. No leak subtraction was applied during recording and reversibility of the block was confirmed by perfusion of bath solution.

Acknowledgements

This work was supported in part by grants from the National Institutes of Health (NS073712 to CB, MWP and RSN; AI084981 to CB). RSN acknowledges fellowship support from the National Health and Medical Research Council of Australia. RH was supported by a T32 Training Grant from the National Institutes of Health (HL007676). CB and MWP are inventors on the patent (WO2006042151A2) describing ShK-186 and analogues. Kineta Inc. (Seattle, WA, USA) has licensed this patent from the University of California and is developing this peptide as a therapeutic for treatment of autoimmune diseases. CB is a consultant to Kineta Inc.

Author contributions

SCC, RH, SC, MWP and BJS performed the experiments. SCC, CB, MWP, BJS and RSN designed the experiments and analyzed the data. SCC, BJS and RSN wrote the article with input from all authors.

References

1 Shapira Y, Agmon-Levin N & Shoenfeld Y (2010) Defining and analyzing geoepidemiology and human autoimmunity. *J Autoimmun* **34**, J168–J177.
2 Moroni L, Bianchi I & Lleo A (2012) Geoepidemiology, gender and autoimmune disease. *Autoimmun Rev* **11**, A386–A392.
3 Walsh SJ & Rau LM (2000) Autoimmune diseases: a leading cause of death among young and middle-aged women in the United States. *Am J Public Health* **90**, 1463–1466.
4 Sallusto F, Geginat J & Lanzavecchia A (2004) Central memory and effector memory T cell subsets: function, generation, and maintenance. *Annu Rev Immunol* **22**, 745–763.
5 Sallusto F, Lenig D, Forster R, Lipp M & Lanzavecchia A (1999) Two subsets of memory T lymphocytes with distinct homing potentials and effector functions. *Nature* **401**, 708–712.
6 Wulff H, Calabresi PA, Allie R, Yun S, Pennington M, Beeton C & Chandy KG (2003) The voltage-gated Kv1.3 K^+ channel in effector memory T cells as new target for MS. *J Clin Invest* **111**, 1703–1713.
7 Beeton C, Wulff H, Standifer NE, Azam P, Mullen KM, Pennington MW, Kolski-Andreaco A, Wei E, Grino A, Counts DR *et al.* (2006) Kv1.3 channels are a therapeutic target for T cell-mediated autoimmune diseases. *Proc Natl Acad Sci USA* **103**, 17414–17419.
8 Fasth AER, Cao D, van Vollenhoven R, Trollmo C & Malmstrom V (2004) $CD28^{null}CD4^+$ T cells - Characterization of an effector memory T-cell population in patients with rheumatoid arthritis. *Scand J Immunol* **60**, 199–208.
9 Friedrich M, Krammig S, Henze M, Docke WD, Sterry W & Asadullah K (2000) Flow cytometric characterization of lesional T cells in psoriasis: intracellular cytokine and surface antigen expression indicates an activated, memory/effector type 1 immunophenotype. *Arch Dermatol Res* **292**, 519–521.
10 Koshy S, Huq R, Tanner MR, Atik MA, Porter PC, Khan FS, Pennington MW, Hanania NA, Corry DB & Beeton C (2014) Blocking Kv1.3 channels inhibits Th2 lymphocyte function and treats a rat model of asthma. *J Biol Chem* **289**, 12623–12632.

11 Lovett-Racke AE, Trotter JL, Lauber J, Perrin PJ, June CH & Racke MK (1998) Decreased dependence of myelin basic protein-reactive T cells on CD28-mediated costimulation in multiple sclerosis patients, A marker of activated/memory T cells. *J Clin Invest* **101**, 725–730.

12 Miyazaki Y, Iwabuchi K, Kikuchi S, Fukazawa T, Niino M, Hirotani M, Sasaki H & Onoe K (2008) Expansion of $CD4^+CD28^-$ T cells producing high levels of interferon-gamma in peripheral blood of patients with multiple sclerosis. *Mult Scler J* **14**, 1044–1055.

13 Rus H, Pardo CA, Hu L, Darrah E, Cudrici C, Niculescu T, Niculescu F, Mullen KM, Allie R, Guo L *et al.* (2005) The voltage-gated potassium channel Kv1.3 is highly expressed on inflammatory infiltrates in multiple sclerosis brain. *Proc Natl Acad Sci USA* **102**, 11094–11099.

14 Viglietta V, Kent SC, Orban T & Hafler DA (2002) GAD65-reactive T cells are activated in patients with autoimmune type 1a diabetes. *J Clin Invest* **109**, 895–903.

15 Vissers WHPM, Arndtz CHM, Muys L, Van Erp PEJ, De Jong EMG & Van de Kerkhof PCM (2004) Memory effector $CD45RO^+$ and cytotoxic $CD8^+$ T cells appear early in the margin zone of spreading psoriatic lesions in contrast to cells expressing natural killer receptors, which appear late. *Br J Dermatol* **150**, 852–859.

16 Corcione A, Casazza S, Ferretti E, Giunti D, Zappia E, Pistorio A, Gambini C, Mancardi GL, Uccelli A & Pistoia V (2004) Recapitulation of B cell differentiation in the central nervous system of patients with multiple sclerosis. *Proc Natl Acad Sci USA* **101**, 11064–11069.

17 Berger T, Rubner P, Schautzer F, Egg R, Ulmer H, Mayringer I, Dilitz E, Deisenhammer F & Reindl M (2003) Antimyelin antibodies as a predictor of clinically definite multiple sclerosis after a first demyelinating event. *N Engl J Med* **349**, 139–145.

18 O'Connor KC, Bar-Or A & Hafler DA (2001) The neuroimmunology of multiple sclerosis: Possible roles of T and B lymphocytes in immunopathogenesis. *J Clin Immunol* **21**, 81–92.

19 Atkinson MA & Eisenbarth GS (2001) Type 1 diabetes: new perspectives on disease pathogenesis and treatment. *Lancet* **358**, 221–229.

20 Dorner T & Burmester GR (2003) The role of B cells in rheumatoid arthritis: mechanisms and therapeutic targets. *Curr Opin Rheumatol* **15**, 246–252.

21 Wulff H, Knaus HG, Pennington M & Chandy KG (2004) K^+ channel expression during B cell differentiation: Implications for immunomodulation and autoimmunity. *J Immunol* **173**, 776–786.

22 Beeton C, Pennington MW & Norton RS (2011) Analogs of the sea anemone potassium channel blocker ShK for the treatment of autoimmune diseases. *Inflamm Allergy Drug Targets* **10**, 313–321.

23 Chi V, Pennington MW, Norton RS, Tarcha EJ, Londono LM, Sims-Fahey B, Upadhyay SK, Lakey JT, Iadonato S, Wulff H *et al.* (2012) Development of a sea anemone toxin as an immunomodulator for therapy of autoimmune diseases. *Toxicon* **59**, 529–546.

24 Wang TG, Lee MH, Johnson T, Allie R, Hu L, Calabresi PA & Nath A (2010) Activated T cells inhibit neurogenesis by releasing granzyme B: rescue by Kv1.3 blockers. *J Neurosci* **30**, 5020–5027.

25 Hu LN, Wang TG, Gocke AR, Nath A, Zhang H, Margolick JB, Whartenby KA & Calabresi PA (2013) Blockade of Kv1.3 potassium channels inhibits differentiation and granzyme B secretion of human $CD8^+$ T effector memory lymphocytes. *PLoS One* **8**, e54267.

26 Wang T, Lee MH, Choi E, Pardo-Villamizar CA, Bin Lee S, Yang IH, Calabresi PA & Nath A (2012) Granzyme B-induced neurotoxicity is mediated via activation of PAR-1 receptor and Kv1.3 channel. *PLoS One*, **7**, e43950.

27 Koch Hansen L, Sevelsted-Møller L, Rabjerg M, Larsen D, Hansen TP, Klinge L, Wulff H, Knudsen T, Kjeldsen J & Köhler R (2015) Expression of T-cell Kv1.3 potassium channel correlates with pro-inflammatory cytokines and disease activity in ulcerative colitis. *J Crohns Colitis* **8**, 1378–1391.

28 Kalman K, Pennington MW, Lanigan MD, Nguyen A, Rauer H, Mahnir V, Paschetto K, Kem WR, Grissmer S, Gutman GA *et al.* (1998) ShK-Dap22, a potent Kv1.3-specific immunosuppressive polypeptide. *J Biol Chem* **273**, 32697–32707.

29 Tudor JE, Pallaghy PK, Pennington MW & Norton RS (1996) Solution structure of ShK toxin, a novel potassium channel inhibitor from a sea anemone. *Nat Struct Biol* **3**, 317–320.

30 Lanigan MD, Kalman K, Lefievre Y, Pennington MW, Chandy KG & Norton RS (2002) Mutating a critical lysine in ShK toxin alters its binding configuration in the pore-vestibule region of the voltage-gated potassium channel, Kv1.3. *Biochemistry* **41**, 11963–11971.

31 Rauer H, Pennington M, Cahalan M & Chandy KG (1999) Structural conservation of the pores of calcium-activated and voltage-gated potassium channels determined by a sea anemone toxin. *J Biol Chem* **274**, 21885–21892.

32 Beeton C, Pennington MW, Wulff H, Singh S, Nugent D, Crossley G, Khaytin I, Calabresi PA, Chen CY, Gutman GA *et al.* (2005) Targeting effector memory T cells with a selective peptide inhibitor of Kv1.3 channels for therapy of autoimmune diseases. *Mol Pharmacol* **67**, 1369–1381.

33 Gilhar A, Bergman R, Assay B, Ullmann Y & Etzioni A (2011) The beneficial effect of blocking Kv1.3 in the psoriasiform SCID mouse model. *J Invest Dermatol* **131**, 118–124.

34 Gutman GA, Chandy KG, Grissmer S, Lazdunski M, Mckinnon D, Pardo LA, Robertson GA, Rudy B, Sanguinetti MC, Stuhmer W *et al.* (2005) International Union of Pharmacology. LIII. Nomenclature and molecular relationships of voltage-gated potassium channels. *Pharmacol Rev* **57**, 473–508.
35 Robbins CA & Tempel BL (2012) Kv1.1 and Kv1.2: similar channels, different seizure models. *Epilepsia* **53** (Suppl 1), 134–141.
36 Coleman SK, Newcombe J, Pryke J & Dolly JO (1999) Subunit composition of Kv1 channels in human CNS. *J Neurochem* **73**, 849–858.
37 Wulff H, Castle NA & Pardo LA (2009) Voltage-gated potassium channels as therapeutic targets. *Nat Rev Drug Discov* **8**, 982–1001.
38 Bagetta G, Nistico G & Dolly JO (1992) Production of seizures and brain damage in rats by α-dendrotoxin, a selective K^+ channel blocker. *Neurosci Lett* **139**, 34–40.
39 Smart SL, Lopantsev V, Zhang CL, Robbins CA, Wang H, Chiu SY, Schwartzkroin PA, Messing A & Tempel BL (1998) Deletion of the Kv1.1 potassium channel causes epilepsy in mice. *Neuron* **20**, 809–819.
40 Glasscock E, Yoo JW, Chen TT, Klassen TL & Noebels JL (2010) Kv1.1 potassium channel deficiency reveals brain-driven cardiac dysfunction as a candidate mechanism for sudden unexplained death in epilepsy. *J Neurosci* **30**, 5167–5175.
41 Adelman JP, Bond CT, Pessia M & Maylie J (1995) Episodic ataxia results from voltage-dependent potassium channels with altered functions. *Neuron* **15**, 1449–1454.
42 Zuberi SM, Eunson LH, Spauschus A, De Silva R, Tolmie J, Wood NW, McWilliam RC, Stephenson JB, Kullmann DM & Hanna MG (1999) A novel mutation in the human voltage-gated potassium channel gene Kv1.1 associates with episodic ataxia type 1 and sometimes with partial epilepsy. *Brain*, **122**(Pt 5), 817–825.
43 Liguori R, Avoni P, Baruzzi A, Di Stasi V & Montagna P (2001) Familial continuous motor unit activity and epilepsy. *Muscle Nerve* **24**, 630–633.
44 Bennett J, Basivireddy J, Kollar A, Biron KE, Reickmann P, Jefferies WA & McQuaid S (2010) Blood-brain barrier disruption and enhanced vascular permeability in the multiple sclerosis model EAE. *J Neuroimmunol* **229**, 180–191.
45 Beeton C, Wulff H, Singh S, Botsko S, Crossley G, Gutman GA, Cahalan MD, Pennington M & Chandy KG (2003) A novel fluorescent toxin to detect and investigate Kv1.3 channel up-regulation in chronically activated T lymphocytes. *J Biol Chem* **278**, 9928–9937.
46 Pennington MW, Beeton C, Galea CA, Smith BJ, Chi V, Monaghan KP, Garcia A, Rangaraju S, Giuffrida A, Plank D *et al.* (2009) Engineering a stable and selective peptide blocker of the Kv1.3 channel in T lymphocytes. *Mol Pharmacol* **75**, 762–773.
47 Tarcha EJ, Chi V, Munoz-Elias EJ, Bailey D, Londono LM, Upadhyay SK, Norton K, Banks A, Tjong I, Nguyen H *et al.* (2012) Durable pharmacological responses from the peptide ShK-186, a specific Kv1.3 channel inhibitor that suppresses T cell mediators of autoimmune disease. *J Pharmacol Exp Ther* **342**, 642–653.
48 Bartok A, Toth A, Somodi S, Szanto TG, Hajdu P, Panyi G & Varga Z (2014) Margatoxin is a non-selective inhibitor of human Kv1.3 K^+ channels. *Toxicon* **87**, 6–16.
49 Mouhat S, Visan V, Ananthakrishnan S, Wulff H, Andreotti N, Grissmer S, Darbon H, De Waard M & Sabatier JM (2005) K^+ channel types targeted by synthetic OSK1, a toxin from *Orthochirus scrobiculosus* scorpion venom. *Biochem J* **385**, 95–104.
50 Varga Z, Gurrola-Briones G, Papp F, de la Vega RCR, Pedraza-Alva G, Tajhya RB, Gaspar R, Cardenas L, Rosenstein Y, Beeton C *et al.* (2012) Vm24, a natural immunosuppressive peptide, potently and selectively blocks Kv1.3 potassium channels of human T cells. *Mol Pharmacol* **82**, 372–382.
51 Eswar N, Webb B, Marti-Renom MA, Madhusudhan MS, Eramian D, Shen MY, Pieper U & Sali A (2006) Comparative protein structure modeling using Modeller. *Curr Protoc Bioinformatics* Chapter 5: Unit 5.6.
52 Liwo A, Oldziej S, Pincus MR, Wawak RJ, Rackovsky S & Scheraga HA (1997) A united-residue force field for off-lattice protein-structure simulations.I. Functional forms and parameters of long-range side-chain interaction potentials from protein crystal data. *J Comput Chem* **18**, 849–873.
53 Berka K, Laskowski RA, Hobza P & Vondrasek J (2010) Energy matrix of structurally important side-chain/side-chain interactions in proteins. *J Chem Theory Comput* **6**, 2191–2203.
54 Pennington MW, Mahnir VM, Khaytin I, Zaydenberg I, Byrnes ME & Kem WR (1996) An essential binding surface for ShK toxin interaction with rat brain potassium channels. *Biochemistry* **35**, 16407–16411.
55 Pohl J, Hubalek F, Byrnes ME, Nielsen KR, Woods A & Pennington MW (1995) Assignment of the three disulfide bonds in ShK toxin: A potent potassium channel inhibitor from the sea anemone *Stichodactyla helianthus*. *Lett Pept Sci* **1**, 291–297.
56 Matheu MP, Beeton C, Garcia A, Chi V, Rangaraju S, Safrina O, Monaghan K, Uemura MI, Li D, Pal S *et al.* (2008) Imaging of effector memory T cells during a delayed-type hypersensitivity reaction and suppression by Kv1.3 channel block. *Immunity* **29**, 602–614.
57 Rashid MH, Heinzelmann G, Huq R, Tajhya RB, Chang SC, Chhabra S, Pennington MW, Beeton C,

Norton RS & Kuyucak S (2013) A potent and selective peptide blocker of the Kv1.3 channel: prediction from free-energy simulations and experimental confirmation. *PLoS One* **8**, e78712.
58 Lepthien S, Hoesl MG, Merkel L & Budisa N (2008) Azatryptophans endow proteins with intrinsic blue fluorescence. *Proc Natl Acad Sci USA* **105**, 16095–16100.
59 Zhang ZW, Alfonta L, Tian F, Bursulaya B, Uryu S, King DS & Schultz PG (2004) Selective incorporation of 5-hydroxytryptophan into proteins in mammalian cells. *Proc Natl Acad Sci USA* **101**, 8882–8887.
60 Shen JY, Chao WC, Liu C, Pan HA, Yang HC, Chen CL, Lan YK, Lin LJ, Wang JS, Lu JF *et al.* (2013) Probing water micro-solvation in proteins by water catalysed proton-transfer tautomerism. *Nat Commun* **4**, 2611.
61 Grabowski H, Long G & Mortimer R (2011) Data exclusivity for biologics. *Nat Rev Drug Discov* **10**, 15–16.
62 Lysandropoulos AP & Du Pasquier RA (2010) Demyelination as a complication of new immunomodulatory treatments. *Curr Opin Neurol* **23**, 226–233.
63 Kingwell E, Koch M, Leung B, Isserow S, Geddes J, Rieckmann P & Tremlett H (2010) Cardiotoxicity and other adverse events associated with mitoxantrone treatment for MS. *Neurology* **74**, 1822–1826.
64 Johnson KP (2010) Risks vs benefits of glatiramer acetate: a changing perspective as new therapies emerge for multiple sclerosis. *Ther Clin Risk Manag* **15**, 153–172.
65 YASARA Biosciences GmbH. YASARA: Yet another scientific artificial reality application. Available: http://www.yasara.org/.
66 Duan Y, Wu C, Chowdhury S, Lee MC, Xiong G, Zhang W, Yang R, Cieplak P, Luo R, Lee T *et al.* (2003) A point-charge force field for molecular mechanics simulations of proteins based on condensed-phase quantum mechanical calculations. *J Comput Chem* **24**, 1999–2012.
67 Chang SC, Galea CA, Leung EWW, Tajhya RB, Beeton C, Pennington MW & Norton RS (2012) Expression and isotopic labelling of the potassium channel blocker ShK toxin as a thioredoxin fusion protein in bacteria. *Toxicon* **60**, 840–850.
68 Grissmer S, Nguyen AN, Aiyar J, Hanson DC, Mather RJ, Gutman GA, Karmilowicz MJ, Auperin DD & Chandy KG (1994) Pharmacological characterization of five cloned voltage-gated K^+ channels, types Kv1.1, 1.2, 1.3, 1.5, and 3.1, stably expressed in mammalian cell lines. *Mol Pharmacol* **45**, 1227–1234.
69 Koshy S, Wu D, Hu X, Tajhya RB, Huq R, Khan FS, Pennington MW, Wulff H, Yotnda P & Beeton C (2013) Blocking KCa3.1 channels increases tumor cell killing by a subpopulation of human natural killer lymphocytes. *PLoS One* **8**, e76740.